HAMILTON COLLEGE

Development of a Compact Bimodal PCB Loop Gap Resonator for High Frequency ESR

by

Leonardo Li

A thesis submitted in partial fulfillment for the
degree of Bachelor of Physics

in the
Department of Physics

Advisor: Professor Charles Collett

February 2026

Abstract

Quantum computing involves the precise control of qubits, one method including manipulation through electron spin resonance (ESR). Bimodal resonators enable independent control of coupled qubits at distinct frequencies, a requirement for implementing two-qubit quantum gates. Achieving reliable ESR requires resonators that generate strong, localized magnetic fields to control spins at multiple frequencies, yet designing compact devices capable of supporting these operating frequencies remains challenging. This thesis investigates resonators constructed with printed circuit board (PCB) material as a scalable and cost effective alternative to conventional loop-gap structures. As a first step, simulations in COMSOL Multiphysics were used to develop a bimodal PCB resonator, which exhibited resonances at 3.8 GHz and 7.9 GHz and demonstrated the feasibility of dual-mode operation. Building on this design, a miniaturized version was developed to meet experimental size constraints. ESR experiments performed this semester using the miniaturized resonator revealed a clear resonance at 3.7 GHz, consistent with simulation, although a second resonant mode has not yet been experimentally identified. A small residual signal was also observed without the sample in place, indicating the possible presence of spin impurities in the PCB material. These results outline both the potential and the unresolved challenges in creating compact, multi-frequency PCB resonators for ESR-based quantum computing systems.

Acknowledgements

Many thanks to Professor Charles Collett for all the guidance and support throughout this project, my fellow researchers over the summer, and Hamilton College for providing the funding that could make this possible.

Contents

List of Figures

Chapter 1

Introduction

Quantum computing has the potential to revolutionize computation by solving problems exponentially faster than classical computers[5]. Realizing this potential, however, depends on the development of scalable, high fidelity systems. Electron spins are very promising due to their well defined quantum states, long coherence times, and fast operational speeds. These spins, often hosted in solid state systems like crystal defects or molecular nanomagnets, function as quantum bits (qubits). The qubit serves as an analog of the bit used in classical computing. Qubits provide advantages over a typical bit by having properties of superposition and entanglement allowing for significantly more computational power. The primary method for controlling these spin qubits is Electron Spin Resonance (ESR), a technique that uses resonant magnetic fields to drive coherent transitions between spin states.

Controlling spin based qubits requires resonators that can efficiently produce oscillating magnetic fields at precise frequencies. Conventional loop gap resonators have been used in previous research[6][7] and have shown to work within experimental constraints. However, the designs of these resonators are very complex and thus pose challenges in manufacturing and implementation. Resonators fabricated on printed circuit board (PCB) material are a possible alternative to standard resonators, but research in this topic is lacking. Current PCB resonator designs use copper traces[8] whereas we hope to construct a LGR geometry on our PCB. This thesis investigates PCB based resonator architectures as an alternative platform.

Because qubits are able to entangle with other qubits, multi-qubit operations in quantum computing require two qubits coupled together. We use molecular nanomagnets[9], spin systems that are chemically engineered to have similar properties as qubits. In order to manipulate multi-qubit systems with ESR, we require different resonant frequencies to control different qubits. Our eventual goal is the fabrication of a loop gap resonator

constructed with PCB material that operates at two different resonant frequencies compatible with our molecular nanomagnet.

In this thesis, we design, simulate, fabricate, and experimentally characterize a compact PCB based LGR for ESR applications. Simulations are employed to develop a bimodal resonator design. The fabricated resonator is tested at cryogenic temperatures using ESR techniques, including frequency sweeps, Hahn echo measurements, and relaxation time analysis. Different coupling configurations are explored to isolate resonant modes and improve signal detection.

Chapter 2

Background Theory

2.1 Qubits

A qubit is similar to a classical bit as both has two different states. There are two types of qubits, spin qubits and superconducting qubits. Electron spin resonance deals with spin qubits. Unlike a classical bit, which has the 0 and 1 states, a spin qubit has spin up and spin down states. The difference is that a qubit has the property of superposition, which means it can be in any linear combination of the two states. In our case, the spins of the electron represents these states in the qubit.

One way to represent the combination of states in the electron is using bra-ket notation. As the electron only has two spin states, using the standard S_z basis, we can represent spin up along the $+z$ axis as $|\uparrow\rangle$ and spin down along the $-z$ axis as $|\downarrow\rangle$. These can also be represented as vectors:

$$|\uparrow\rangle = \begin{bmatrix} 1 \\ 0 \end{bmatrix}, |\downarrow\rangle = \begin{bmatrix} 0 \\ 1 \end{bmatrix}. \tag{2.1}$$

Any generic spin can be represented as a linear combination of these vectors:

$$|\psi\rangle = \alpha\,|\uparrow\rangle + \beta\,|\downarrow\rangle\,, \tag{2.2}$$

where $\alpha^2 + \beta^2 = 1$. Visually, these states can be represented by the Bloch sphere, where the spin up configuration is shown in Figure 2.1.

Electron spins are particularly attractive for quantum computing due to their long coherence times (microseconds to milliseconds), fast gate operation speeds (nanoseconds), and manipulation techniques through ESR.

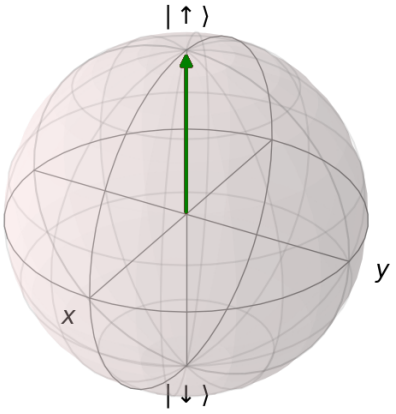

Figure 2.1: Bloch sphere representation of $|\psi\rangle = |\uparrow\rangle$.

2.1.1 Molecular Nanomagnets

Molecular Nanomagnets are a special class of molecule that can be chemically engineered to alter the spin Hamiltonian whose spins can be used as memory qubits[6].

In our desired quantum computing qubit, we use a dimer, two connected molecules of Cr_7Mn, which allows for coupling between each molecule as each individual molecule can function as a qubit. Thus the Cr_7Mn dimer functions as a natural 2 qubit system. We work with two variants of Cr_7Mn, each with a different resonant frequency found to be around 4 and 5.3 GHz[7].

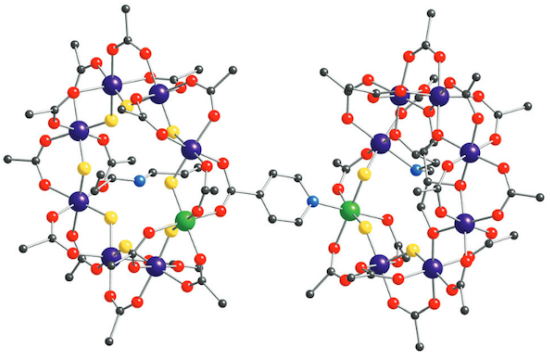

Figure 2.2: Illustration of a similar dimer, consisting of a pair of Cr_7Ni system of molecules[1]

2.2 Electron Spin Resonance

To interact with spins, we can apply an oscillating magnetic field to drive transitions between the two spin states. A clear transition from one state to another, for example from $|\uparrow\rangle$ to $|\downarrow\rangle$, is called coherent. An electron in a strong magnetic field B_0 applied

along z has Hamiltonian

$$H_0 = g\mu_B B_0 S_z, \tag{2.3}$$

with μ_B being the Bohr magneton and $g \approx 2.0023$ as the electron g-factor in a vacuum. The Hamiltonian represents the total energy in the system. If we assume the field aligns all spins in either $|\uparrow\rangle$ or $|\downarrow\rangle$ configurations, then the energy levels of the electron are

$$E_+ = \frac{1}{2} g\mu_B B_0, E_- = -\frac{1}{2} g\mu_B B_0. \tag{2.4}$$

The oscillating magnetic field is able to drive a transition between spin states when the frequency matches the energy gap:

$$\hbar\omega = E_+ - E_-. \tag{2.5}$$

This frequency ω is the resonant frequency.

2.2.1 Spin Echoes

In order to detect these spins, we use a method of radiofrequency (RF) pulse sequences to manipulate and characterize spins. Given our two state system, we start with most spins in the relaxed state of $|\uparrow\rangle$. Then, a $\frac{\pi}{2}$, or 90°, pulse is applied using a magnetic field to tip the spins into the transverse plane. From here, the spins begin to precess in the transverse plane, but due to small inconsistencies, each spin precesses at a different frequency, and thus go from coherent (all spins aligned and rotating together in the same direction) to dephased (losing their synchronization and no longer rotating in unison). After τ time, a π or 180° pulse is applied which flips the spins and the precession direction of the spins. This forces the spins to precess back into the initial coherent configuration, when all the spins are aligned. When all the spins are aligned, they can produce a measurable field which is called the spin echo. This is an example of the Hahn echo experiment, which is the most simple ESR spin echo experiment.

When spins are in an excited state, they will slowly lose energy to return to the relaxed state. The time it takes the spins to return to their relaxed states is called the relaxation time. There are two relaxation times for spins. The first is called spin-lattice relaxation, denoted by T_1. This is given by the time it takes for the spins to go completely back to the original relaxation state, and is usually much longer than T_2. The second relaxation time is called spin-spin relaxation (T_2), which is given by the time it takes for precession in the transverse plane to go completely out of phase.

2.2.2 Calculating Relaxation Times

Calculating spin-spin relaxation is fairly simple. Because the strength of the echo in the Hahn echo experiment decays exponentially with time, we can model it as

$$M(t) = M_0 e^{\frac{-t}{T_2}}, \tag{2.6}$$

where M is the measured signal strength, M_0 is the initial pulse strength, and t is the time between the initial 90° pulse and the echo, or 2τ.

On the other hand, calculating spin-lattice relaxation is more complicated and requires a new method called the inversion recovery experiment. We first apply a π pulse to invert the spin, then while the spin relaxes, we apply periodic Hahn echoes to obtain a snapshot of the signal strength at that moment while the spins relax. Modeling these signals over time gives us the equation

$$M(t) = M_0(1 - 2e^{\frac{-t}{T_1}}). \tag{2.7}$$

2.3 Resonators

ESR experiments require oscillating magnetic fields in order to drive coherent transitions in spin states. These magnetic fields can be created in structures called resonators. We will work with a certain type of resonator called a loop gap resonator (LGR). An LGR can be modeled as a lumped RLC circuit where the electric and magnetic fields are contained within separate parts of the structure. The electric field is contained in the gap of the resonator that functions as the capacitator plates, while the inductor is the loop which contains the magnetic field. A simple LGR is shown in figure 2.3.

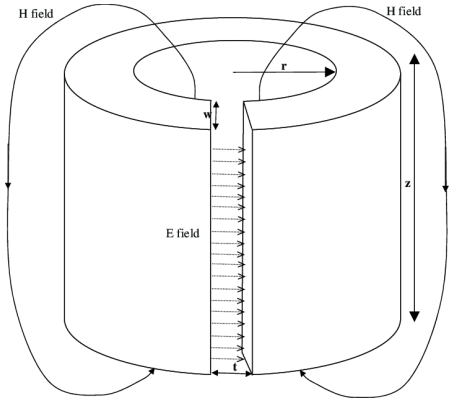

Figure 2.3: A diagram of a simple LGR showing the electric and magnetic fields [2].

For a simple LGR, the capacitance and inductance are as follows[10]:

$$C = \epsilon_r \epsilon_0 \frac{(w+t)(z+t)}{nt} \tag{2.8}$$

$$L = \frac{\mu_0 \pi r^2}{z + 0.9r}, \tag{2.9}$$

where w = width of gap, n = number of gaps, ϵ_0 is the permittivity of free space, ϵ_r is the dielectric constant of the gap, z = length of loop and gap, t = thickness of gaps, μ_0 is the permeability of free space, and r = radius of loop.

The capacitance and inductance give us the resonant frequency of the resonator,

$$f_0 = \frac{1}{2\pi\sqrt{LC}}. \tag{2.10}$$

The quality factor is given by

$$Q_L = \frac{f_0}{\Delta f}, \tag{2.11}$$

where Δf is full width at half maximum intensity. The quality factor describes the ringdown after an RF pulse where the resonator will oscillate with energy. The time constant of a ringdown is:

$$T_R = \frac{Q_L}{2\pi f}. \tag{2.12}$$

Typically, a shorter ringdown is preferred when dealing with ESR due to interference from ringdown signal when trying to detect spins.

2.3.1 Resonator Coupling

A resonator by itself isn't enough to produce the magnetic fields for ESR. To transfer power between the resonator and external circuits, energy must be coupled through interaction with the resonator's electromagnetic fields. The two primary coupling methods are inductive and capacitive coupling.

Capacitive coupling occurs through electric field interaction. A coupling probe or electrode is positioned in a region of high electric field within the resonator. For LGRs, this is near the gap of the resonator where the electric field is concentrated. The probe and resonator structure form a capacitor, allowing energy transfer. When an oscillating voltage is applied to the probe, the resulting electric field will also oscillate, inducing displacement currents within the resonator, exciting the resonant mode.

Inductive coupling occurs through magnetic field interaction. A coupling loop, like capactive coupling, is positioned in a region of high magnetic field. An oscillating current

is driven through the loop, generating magnetic flux that passes through the resonators inductive loop. By Faraday's law, the changing flux induces currents in the resonator. Inductive coupling is strongest when the loop is positioned to maximize flux through the resonator, typically within or adjacent to the resonator loop.

2.4 PCB Resonators

While conventional LGRs are typically fabricated from machined metals like copper, PCB technology offers an alternative fabrication approach with advantages for ESR application.

PCB resonators can be fabricated using CNC milling or photolithographic etching. An LGR design is transferred to PCB material where unwanted copper is removed, leaving the resonator structure on one side and coupling structures, such as antennas, on the other. CNC milling lets us test designs extremely quickly compared to chemical processes. A design can be milled and ready to test within hours. Additionally, the low per unit cost of these resonators and accessibility of milling machines means optimization of resonators is highly efficient.

Chapter 3

Experimental Setup

3.1 Cryostat

To reduce environmental interference on qubits by heat and outside noise, all ESR experiments are conducted at very low temperatures inside of an SHI-950T cryostat from Lake Shore cryotronics, shown in figure 3.1.

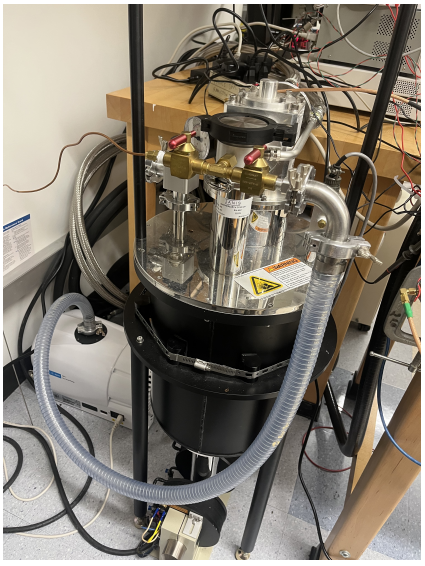

Figure 3.1: Cryostat used for ESR.

The cryostat pumps helium to cool down and can run indefinitely at 3K. Additionally, it can cool down to 1.5K for short periods of time for ESR experiments at lower temperatures.

3.2 Sample Probe

The sample probe is our main method of getting the sample inside the cryostat, inserted from the top. It consists of several long G10? rods for stability, with a shielded sample chamber on one end and linear adjustable micrometer mechanisms on the other end. The full apparatus is shown in figure 3.2.

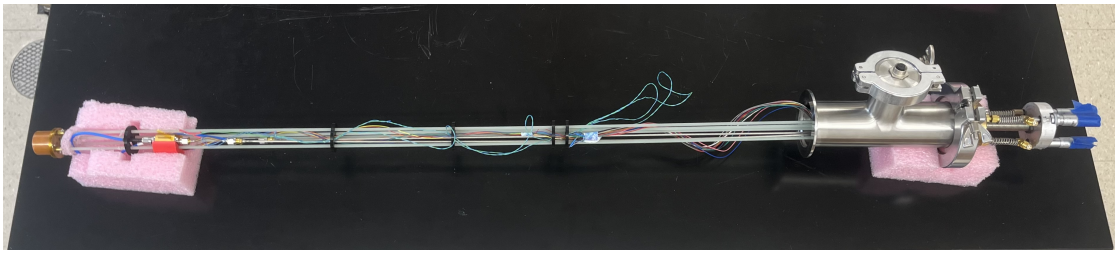

Figure 3.2: Full sample probe setup.

The shielded sample chamber is made up of a cylindrical copper shield with a copper cap on both sides. The bottom cap has screw holes for mounting resonators, and the top cap has holes to allow for antennas to enter the chamber. These components are shown in figure 3.3.

Figure 3.3: Components of the shielded sample chamber.

3.2.1 Antenna setup

A capacitive antenna is created from a normal shielded coax cable, and approximately 1-2 cm of outer coax is stripped away at one end, which exposes the inner conductive wire. This wire is bent 90° and the antenna is inserted through a hole in the top cap and positioned over a gap in the mounted resonator.

Figure 3.4: End of the capacitive antenna, showing the stripped coax.

The inductive antenna is built into the resonator. To get current in the antenna, wires are soldered to each end of the inductive loop and the wires are ran through the top cap, to another coax with a stripped end. One wire is soldered to the inside wire of the coax, and the other wire is soldered to the grounded outer shell of the coax.

Both coax cables are connected to the linear adjustable mechanism on the top of the sample probe. This allows micrometer adjustments of the separation of the capacitive antenna from the resonator, allowing for tuning while inside the cryostat.

3.2.2 Resonator mount

The solder and wiring on the underside of the resonator means that it cannot be mounted directly to the bottom cap of the shield. A 3-D printed support mount is placed underneath the resonator to separate the shield surface from wire connections on the resonator. Figure 3.5 shows the mounting setup for the resonator.

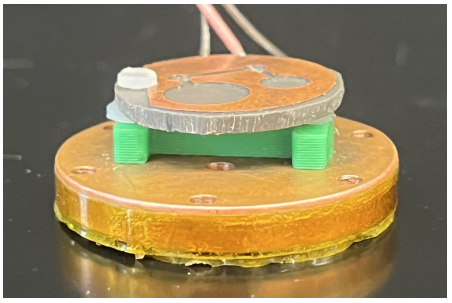

Figure 3.5: Setup to mount the resonator.

3.3 Spectrometer and Network Analyzers

In order to perform ESR and detect signals, we need to be able to send pulses down our antennas and detect responses. This can be accomplished through the use of a spectrometer, specifically one designed by Collett et al[11].

For quick adjustment and tuning of antennas, we instead use a Vector Network Analyzer (VNA). VNAs are handheld devices that can measure signals being reflected in an antenna. So in order to get the capacitive antenna into position or for a basic check for signal from the inductive antenna, we use the VNA and from there all experiments are done with the spectrometer.

Figure 3.6: Example of signal detected using a VNA.

Chapter 4

Methods

4.1 Resonator Design

The bimodal LGR design was inspired by the works of Libersky et al[3], who demonstrated a LGR supporting resonant modes at around 1.8 and 3 GHz. This resonator design is shown in figure 4.1.

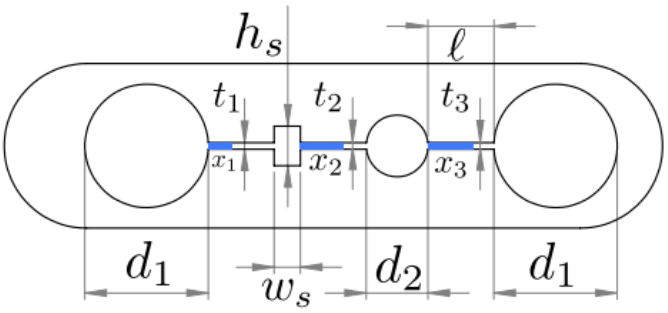

Figure 4.1: Illustration of the resonator used by Libersky et al[3].

This basic design was then modeled on a PCB surface in COMSOL Multiphysics within a shield and capacitive coupled antenna. Because the design was too elongated to theoretically fit within a circular sample probe, a process of trial and error with redesigning the geometry of the various gaps and loops yielded a working bimodal design by David Reyes shown in figure 4.2.

Due to the design being based off the dimensions found by Libersky et al, the size was much larger than the interior of the sample probe. This required another long process of trial and error to shrink the resonator to be able to fit within the sample probe and have the desired resonant frequencies. On the other side of the PCB a coupling loop was

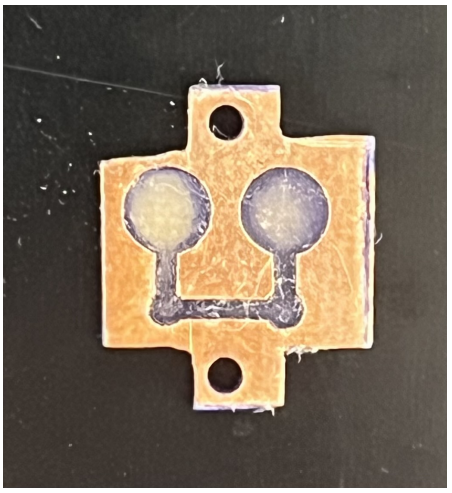

Figure 4.2: Working bimodal resonator design by David Reyes[4]

designed and tested through simulation software and resonant frequencies with magnetic fields were found.

The final resonator design included removing a small strip of copper off of the resonator, allowing a hole to be drilled to allow mounting to the sample probe.

4.1.1 Resonator Fabrication

Initial variants of the PCB resonator were milled on FR-4 substrate PCB material. The final version of the resonator was milled on FR-6 substrate PCB material. The fabrication process required recreating the resonator design in CAD software (Autodesk Fusion) and creating a milling program in Fusion. The PCB design is then milled onto precut blanks of PCB material. Then, the circular PCB is cut out from the blank and sanded in the shop.

4.2 Setting up for ESR

The resonator is mounted onto the bottom shield cap, and a small sample tube of of Cr_7Mn is coated with grease to prevent movement and placed into the hole in the resonator loop. In some cases where the resonator will undergo frequent periods of warming up and cooling down, we use borosilicate glass due to its stability when experiencing temperature changes. In those cases a small shard of borosilicate glass has grease applied to a flat side and placed on the loop of the resonator.

Once the sample is in place, the shield assembly is screwed together. The capacitive antenna is carefully positioned by using the VNA to determine an initial coupling at

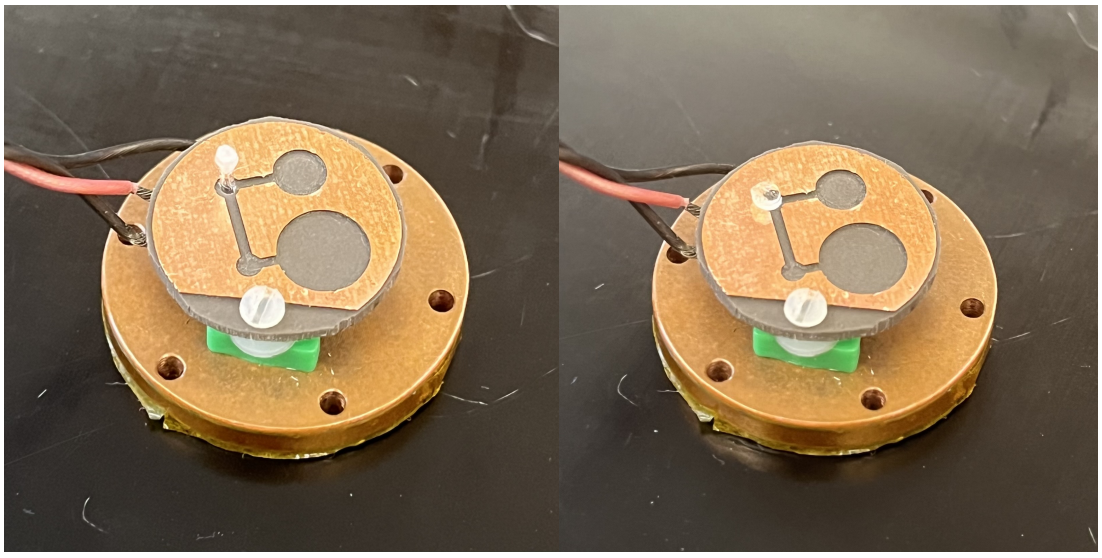

(a) (b)

Figure 4.3: Sample of Cr_7Mn in resonator (a) and sample of borosilicate in resonator (b)

room temperature. This is done by adjusting the antenna until a reflection signal can be seen on the VNA. Once a coupling is found, the sample probe setup is carefully lowered into the cryostat and sealed. Helium is then pumped and flushed to bring the cryostat down to temp.

Once the cryostat reaches operating temperatures (around 3K), the VNA is again used to determine if any changes to the coupling between the antenna and the LGR has occurred. Once the coupling is determined, the resonator setup is ready for ESR testing.

4.3 Characterization using ESR

When the resonator is ready for ESR, the inductive antenna is connected to the spectrometer. Because the VNA only gives a rough approximation to where resonant modes could be, a frequency sweep from the spectrometer is able to detect possible resonant modes with much higher levels of precision. From the frequency sweep we can determine possible resonant frequencies. Usually many peaks will appear, but most are caused by cavity modes or parasitic modes. The best method to determining if a frequency is actually the resonant frequency, we can perform Hahn echoes at those frequencies. If the frequency is at resonance, then the Hahn echo will interact with the spins and produce a signal. To minimize background noise, the Hahn echo experiments are performed thousands of times and averaged for the most accurate results.

If a signal is found, then we can calculate T_1 and T_2 relaxation times from Hahn echo and inversion sweep experiments. These times can then be compared with previous results from normal LGRs.

4.3.1 Characterization with different couplings

Another method we employed could possibly find the resonant frequency much more efficiently than the approach described in 4.3. In this method, we perform a frequency sweep using the inductive antenna and the capacitive antenna independently. Peaks that appear in similar frequencies in both antennas are more indicative of a possible resonant frequency.

4.3.2 Transmission coupling mode

Taking the idea for 4.3.1 a step further, we can perform frequency sweeps and ESR by using one of the two antennas as a transmitter and the other as a reciever. This requires some changes to the spectrometer setup, but can reduce noise and reflections even further as the receiving antenna does not send signal down to the resonator, only transmitting signal from the resonator. The receiver antenna was determined from analysis of frequency sweeps performed by each antenna. The one with the stronger detected peaks, also a sign of better coupling, was used as the receiver. This method is able to be used in ESR and is shown to give clearer results, discussed later in the paper.

Chapter 5

Results

5.1 PCB Resonator

The final design for the PCB resonator that we test for resonant frequencies is shown in figure 5.1. COMSOL simulations showed resonances at 4.43 and 6.88 GHz.

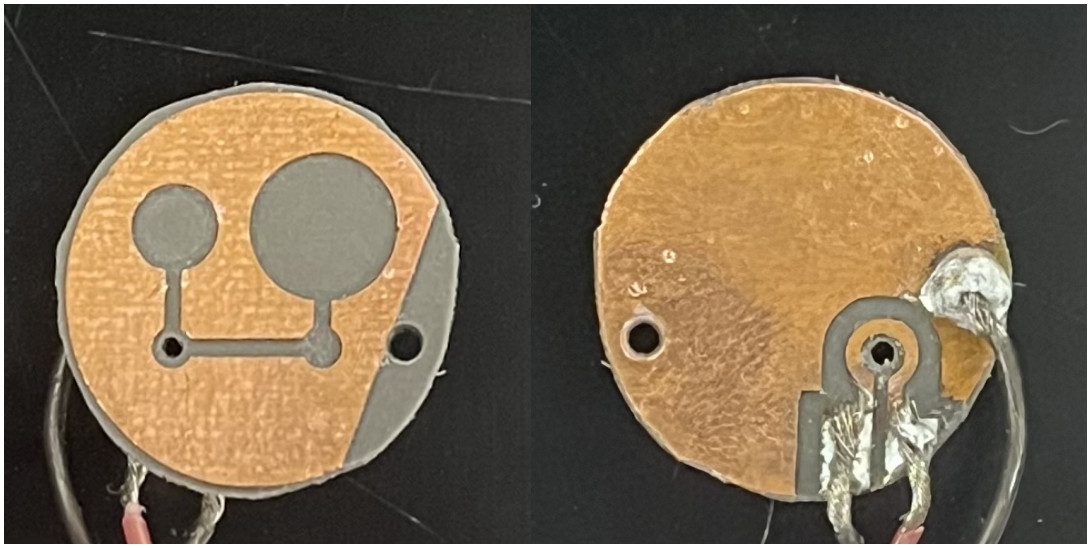

(a) (b)

Figure 5.1: Top side (a) and bottom side (b) of resonator.

5.2 Initial Measurements

Initial frequency sweeps of the resonator were conducted with the inductive antenna at 3K on a sample of borosilicate. This frequency sweep yielded many potential resonances.

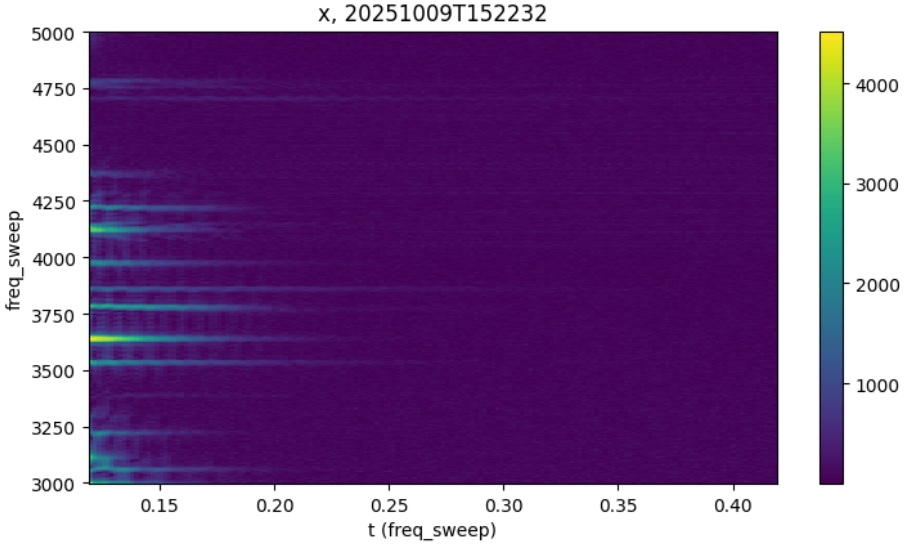

Figure 5.2: Frequency sweep conducted with the inductive antenna at 3-5 GHz.

Hahn echo experiments at the strongest peaks yielded no signal.

5.3 Comparing Peaks

Using the method from 4.3.1, a frequency sweep using the capacitive antenna and inductive antenna were ran at 3K and the resulting peaks analyzed.

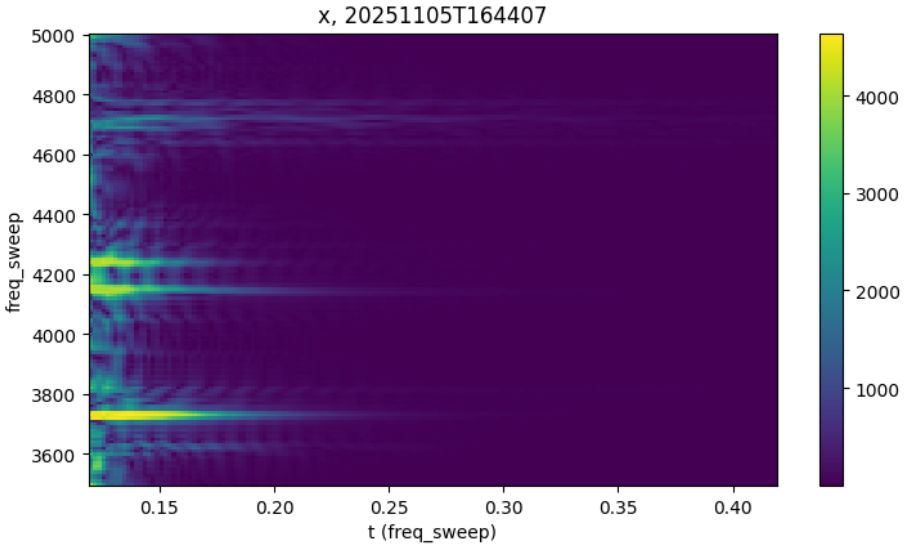

Figure 5.3: Frequency sweep conducted with the inductive antenna at 3.5-5 GHz

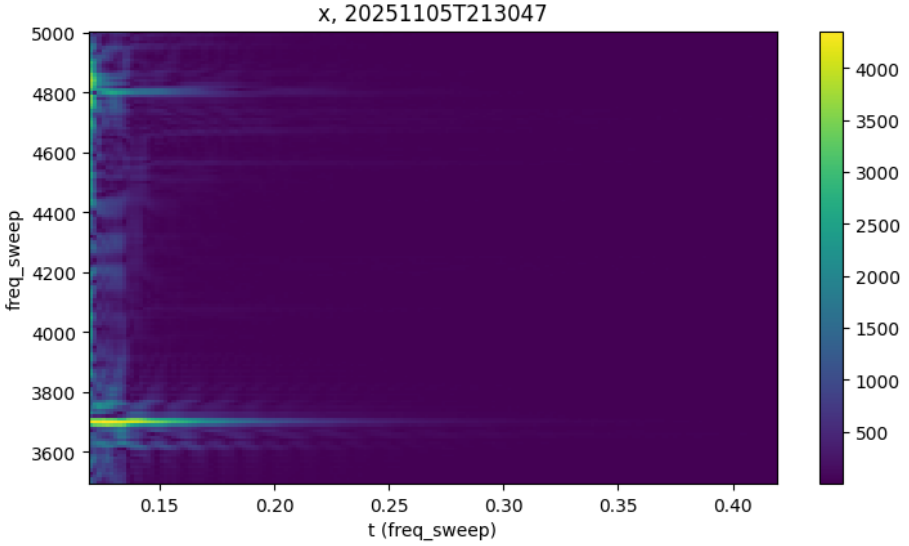

Figure 5.4: Frequency sweep conducted with the capacitive antenna at 3.5-5 GHz

Both frequency sweeps showed a promising peak at approximately 3.7 GHz. However, Hahn echo experiments at 3.7 for each antenna did not show any signal.

5.4 Transmission Mode Hahn Echo

The result from 5.3 led us to implementing the transmission mode method described in 4.3.2. After analyzing a sweep around 3.7 GHz from both antennas, the inductive antenna was determined to be the receiver. Figure 5.5 shows the stronger signal from the inductive antenna compared to the capacitive one.

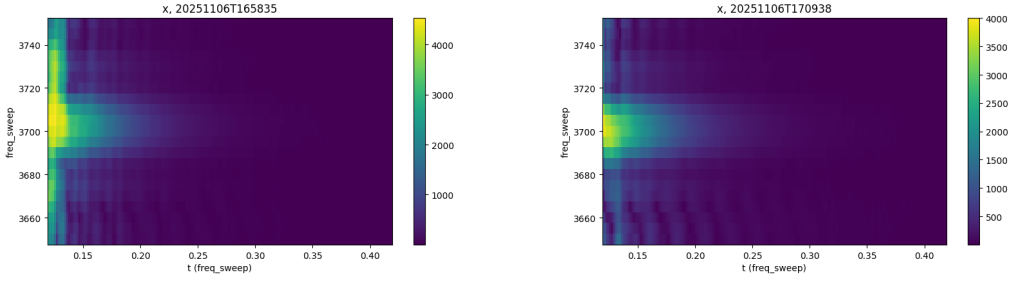

(a) (b)

Figure 5.5: Signal at 3.7 GHz of the inductive antenna (a) and the capacitive antenna (b)

The sweep around 3.7 GHz in transmission mode showed a clear signal with little noise.

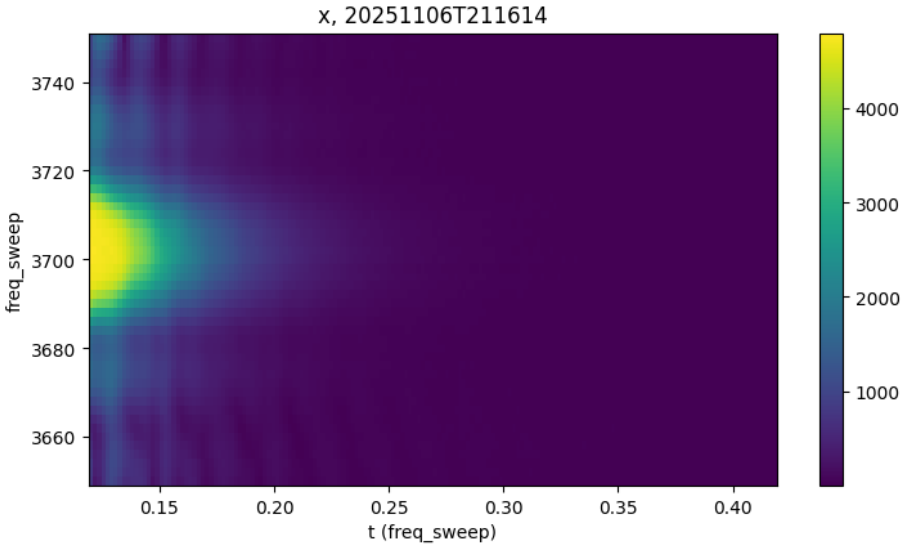

Figure 5.6: Signal at 3.7 GHz in transmission mode.

With this result, we began performing Hahn echoes with different pulse lengths to search for a signal. Signal was found with the pulse setup in figure 5.7.

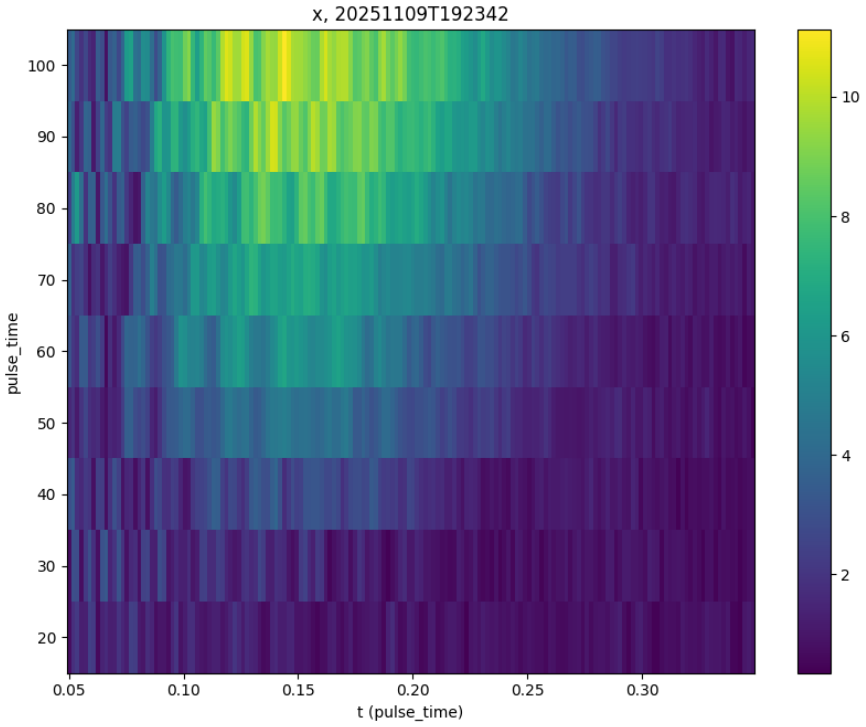

Figure 5.7: Hahn echo signal at 3.7 GHz using 500 ns delay, 40 ns pulse time, 250 μs repetition time.

5.5 Relaxation Times

Fitting the Hahn echo data from figure 5.7 to the T_2 relaxation equation found a T_2 time of 810 ns.

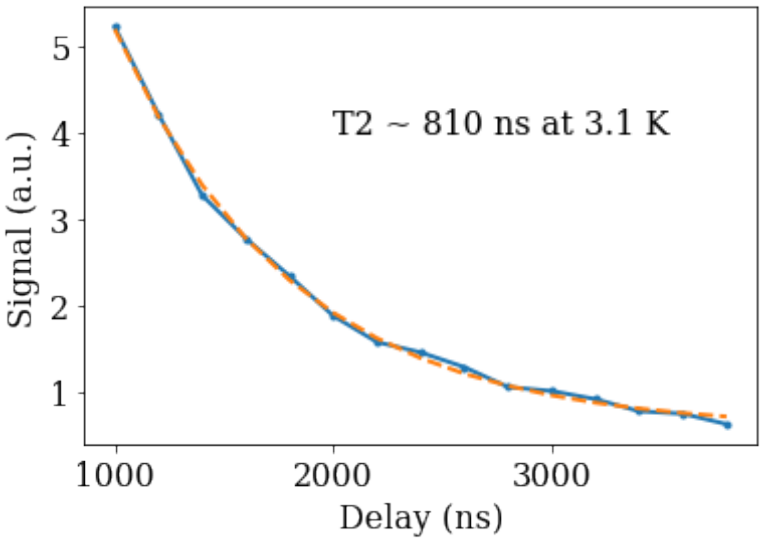

Figure 5.8: Hahn echo T_2 decay fit.

An inversion sweep with fit found a T_1 time of 80 μs.

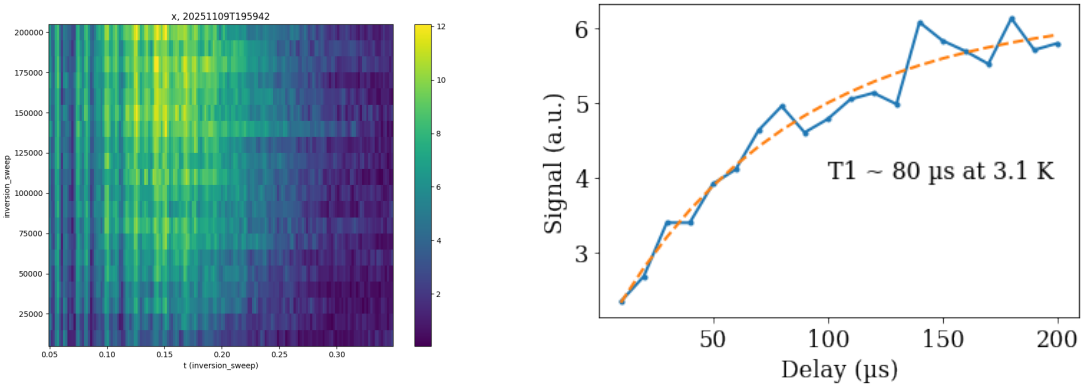

(a) (b)

Figure 5.9: Inversion sweep (a) and corresponding T_1 fit.

Another Hahn echo performed with just the inductive antenna with 20000 averages and 4 repetitions showed it is possible to see signal without using transmission mode, although the signal is very weak and required 3 more repetitions.

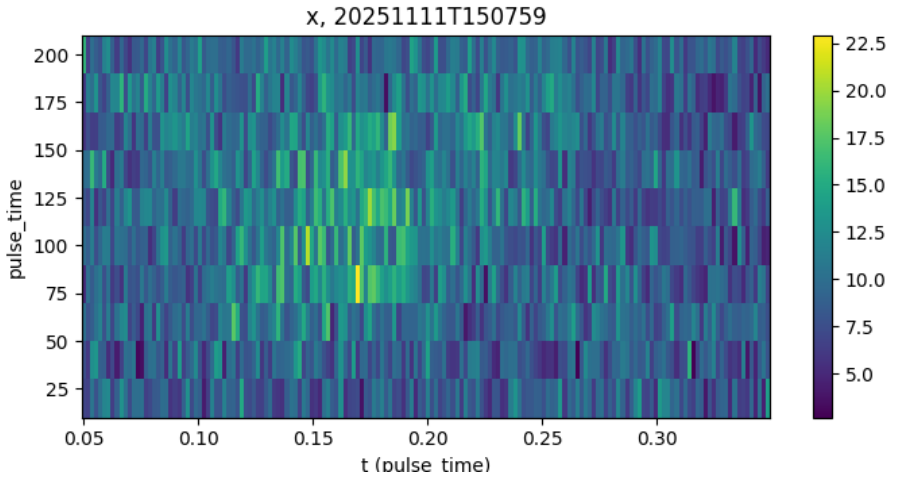

Figure 5.10: Hahn echo signal with the inductive antenna

These results are consistent with a resonant frequency at 3.7 GHz.

5.6 Locating the Field

With these results, it is necessary to verify if the magnetic field from the resonant mode is actually contained within the loop we want. This is because there is a possibility we are seeing a resonance from the PCB substrate or other factors. To verify, we first checked if the Hahn echo signal was present if every loop had borosilicate in them, then removed a piece one by one.

As expected, with borosilicate in every loop, we saw a signal. Since simulations showed little to no magnetic fields within the larger loops, we decided to speed up the process by removing both pieces from the larger loops. Hahn echo performed with this setup also showed signal. Additionally, a Hahn echo was performed while the sample was under an external magnetic field of 300 gauss. The signal strength was decreased to little or no response.

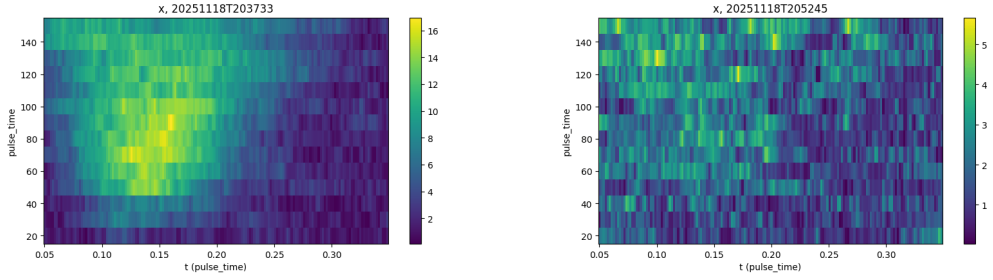

(a) (b)

Figure 5.11: Hahn echo with two borosilicate samples (a) and Hahn echo under magnetic field (b)

Next, the borosilicate in the loop that didn't have a field in the simulations was removed. If this showed a signal, then that loop could be ruled out as containing the magnetic field. Similar to the Hahn echo with two borosilicate samples, the Hahn echo was also run under a 300 gauss external magnetic field.

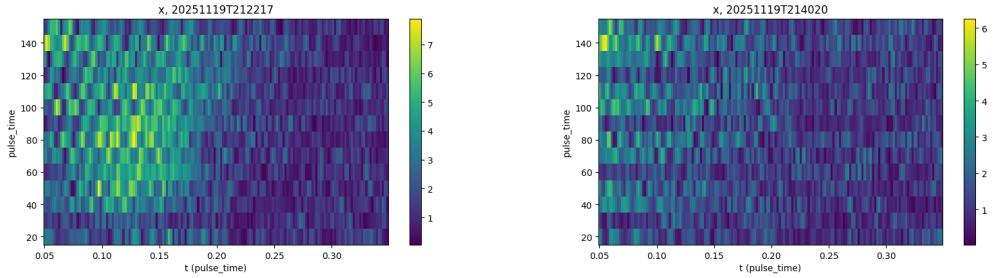

(a) (b)

Figure 5.12: Hahn echo with one borosilicate sample (a) and Hahn echo under magnetic field (b)

Finally, a Hahn echo was run with no borosilicate samples present.

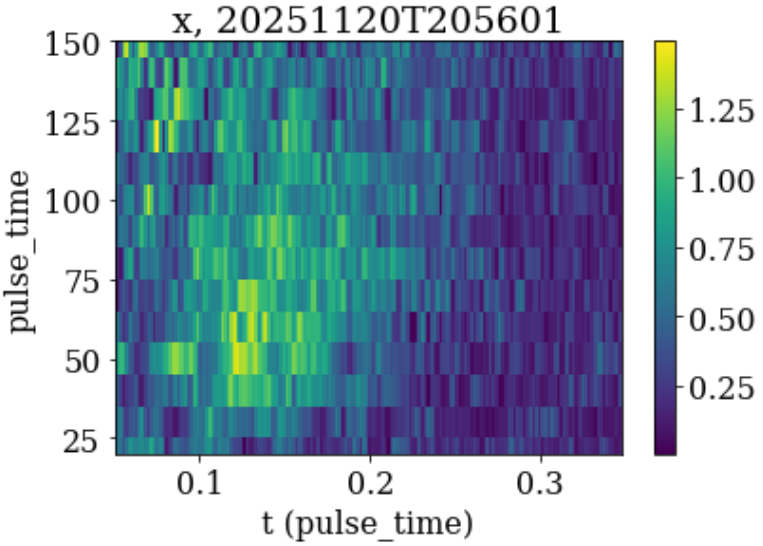

Figure 5.13: Hahn echo with no samples

Chapter 6

Discussion and Conclusion

The primary goal of this work was to investigate if PCB-based LGRs can support resonant modes suitable for ESR experiments, possibly at multiple frequencies for multi-qubit control. COMSOL simulations predicted two resonant modes in the final resonator design, and ESR experiments successfully identified a resonance at 3.7 GHz. Using transmission mode coupling, strong echo signals allowed us to calculate relaxation times. The measured values of $T_1 \approx 80$ μs and $T_2 \approx 810$ ns are consistent with previous results from the lab. This indicates that the PCB resonator can effectively generate and confine the desired oscillating magnetic fields.

The experimentally observed resonance at 3.7 GHz is a slight deviation from the predicted COMSOL simulation, where a resonance was found at 4.43 GHz. Considering uncertainties in fabrication tolerances, coupling conditions inside the shielded sample chamber, as well as a slight change in the design to be able to mount to the shield, we can reasonably expect a possible shift in resonance. The absence of a clearly identifiable second resonant mode in ESR experiments, despite its presence in simulations, suggests that the higher-frequency mode may suffer from weaker magnetic field confinement, reduced coupling efficiency, or increased losses in the PCB material.

Additionally, the appearance of multiple peaks in initial frequency sweeps highlights the challenge of distinguishing true resonator modes from cavity or parasitic modes. The comparison of inductive and capacitive coupling, and especially the implementation of transmission-mode ESR, were beneficial for isolating the relevant resonance.

Systematic removal of borosilicate samples from different loops provided further evidence that the observed ESR signal originates from the intended resonator loop rather than from the PCB substrate or surrounding cavity. The strong suppression of the Hahn echo signal under an external magnetic field further supports the conclusion that the detected

signal is due to spin resonance rather than other factors. Together, these tests confirm that the 3.7 GHz mode corresponds to a magnetic field localized within the specified loop.

However, a weak echo-like signal was also observed when no sample was present in the resonator. This background response could be due to impurities or defect spins in surrounding materials such as the PCB substrate, copper surfaces, grease, or leftover borosilicate from previous experiments. Most importantly, the magnitude and visibility of the echo depended on sample placement and was strongly suppressed under an applied static magnetic field, indicating that the observed response is not purely an instrumental artifact. These observations suggest that while background spins contribute to the detected signal, the primary resonance at 3.7 GHz is consistent with ESR driven by the resonator's localized magnetic field.

Despite the successful observation of ESR, several limitations remain. Most notably, the second resonant mode predicted by simulations was not experimentally observed. Possible explanations include increased dielectric losses at higher frequencies or insufficient coupling strength. Another concern is that the resonant frequency found may not work with the molecular nanomagnet. Possible solutions could involve methods to increase the resonant frequency including adding a dielectric to a gap.

This work demonstrates that PCB-based LGRs can be miniaturized and still support ESR at cryogenic temperatures. Future work should focus on trying to locate the higher frequency resonant mode, whether through more ESR experiments while changing pulse lengths or repetition times, or designing a new resonator with a more prominent simulated higher frequency mode. Determining the second resonant frequency would allow for multi-qubit ESR experiments.

Bibliography

[1] Grigore Timco, Simone Marocchi, Elena Garlatti, Claire Barker, Morten Albring, Valerio Bellini, Franca Manghi, Eric J. L. McInnes, Robin G. Pritchard, Floriana Tuna, Wolfgang Wernsdorfer, Giulia Lorusso, Giuseppe Amoretti, Stefano Carretta, Marco Affronte, and Richard E. P. Winpenny. Heterodimers of heterometallic rings. *Dalton Trans.*, 45:16610–16615, 2016.

[2] https://www.researchgate.net/profile/Aharon-Blank/publication/47632846/figure/fig8/AS:667039823822855@1536046095604/Typical-conventional-metallic-loop-gap-resonator.png.

[3] Matthew M. Libersky, Daniel M. Silevitch, and Ammar Kouki. Design of a loop-gap resonator with bimodal uniform fields using finite element analysis, 2019.

[4] David Reyes. Personal communication, 2025.

[5] Josh Schneider and Ian Smalley. What is quantum computing? https://www.ibm.com/topics/quantum-computing, August 2024.

[6] Charles A. Collett, Paolo Santini, Stefano Carretta, and Jonathan R. Friedman. Constructing clock-transition-based two-qubit gates from dimers of molecular nanomagnets. *Physical Review Research*, 2(3), August 2020.

[7] Peter Jones. *Characterization of Heterodimer of Cr7Mn Using Custom Loop Gap Resonators.* Undergraduate thesis, Hamilton College, Clinton, NY, 2025.

[8] Kerui Li, Jiayang Wu, Abdulkadir C. Yucel, and Shu-Yuen Ron Hui. New printed-circuit-board resonators with high quality factor and transmission efficiency for mega-hertz wireless power transfer applications. *IEEE Transactions on Power Electronics*, 38(10):13207–13218, 2023.

[9] A. Chiesa, P. Santini, E. Garlatti, F. Luis, and S. Carretta. Molecular nanomagnets: a viable path toward quantum information processing? *Reports on Progress in Physics*, 87(3):036501, 2024.

[10] Lawrence J. Berliner Sandra S. Eaton, Gareth S. Eaton. *Biomedical EPR Part B: Methodology, Instrumentation, and Dynamics*. Kluwer Academic, 2005.

[11] Charles A. Collett, Sofia M. Davvetas, Abdulelah Alsuhaymi, and Grigore A. Timco. An inexpensive, configurable two-tone electron spin resonance spectrometer, 2024.